AGU PUBLICATIONS

Geophysical Research Letters

RESEARCH LETTER
10.1002/2017GL076809

Key Points:
- Energy conversion is highly localized within asymmetric reconnection electron diffusion regions
- Oscillatory reconnection electric fields show characteristics of both spatial structures and propagating waves that are consistent with standing oblique quasi-electrostatic whistlers
- Both positive and negative values of $\mathbf{J} \cdot \mathbf{E}$ result from uniform current and oscillating electric fields

Correspondence to:
J. L. Burch,
jburch@swri.edu

Citation:
Burch, J. L., Ergun, R. E., Cassak, P. A., Webster, J. M., Torbert, R. B., Giles, B. L., et al. (2018). Localized oscillatory energy conversion in magnetopause reconnection. *Geophysical Research Letters*, *45*, 1237–1245. https://doi.org/10.1002/2017GL076809

Received 14 DEC 2017
Accepted 23 JAN 2018
Accepted article online 29 JAN 2018
Published online 10 FEB 2018

Localized Oscillatory Energy Conversion in Magnetopause Reconnection

J. L. Burch[1], R. E. Ergun[2], P. A. Cassak[3], J. M. Webster[4], R. B. Torbert[1,5], B. L. Giles[6], J. C. Dorelli[6], A. C. Rager[6,7], K.-J. Hwang[1], T. D. Phan[8], K. J. Genestreti[9], R. C. Allen[10], L.-J. Chen[11], S. Wang[11], D. Gershman[6], O. Le Contel[12], C. T. Russell[13], R. J. Strangeway[13], F. D. Wilder[2], D. B. Graham[14], M. Hesse[15], J. F. Drake[11], M. Swisdak[11], L. M. Price[11], M. A. Shay[16], P.-A. Lindqvist[17], C. J. Pollock[18], R. E. Denton[19], and D. L. Newman[2]

[1]Southwest Research Institute, San Antonio, TX, USA, [2]LASP, University of Colorado Boulder, Boulder, CO, USA, [3]Department of Physics and Astronomy, West Virginia University, Morgantown, WV, USA, [4]Department of Physics and Astronomy, William Marsh Rice University, Houston, TX, USA, [5]Department of Physics, University of New Hampshire, Durham, NH, USA, [6]NASA Goddard Space Flight Center, Greenbelt, MD, USA, [7]Department of Physics, Catholic University of America, Washington, DC, USA, [8]Space Sciences Laboratory, University of California, Berkeley, CA, USA, [9]Space Research Institute, Austrian Academy of Sciences, Graz, Austria, [10]The Johns Hopkins University Applied Physics Laboratory, Laurel, MD, USA, [11]Department of Astronomy, University of Maryland, College Park, MD, USA, [12]Laboratoire de Physique des Plasmas, CNRS, Ecole Polytechnique, UPMC Univ Paris 06, University Paris-Sud, Observatoire de Paris, Paris, France, [13]Department of Earth and Planetary Sciences, University of California, Los Angeles, CA, USA, [14]Swedish Institute of Space Physics, Uppsala, Sweden, [15]Department of Physics and Technology, University of Bergen, Bergen, Norway, [16]Department of Physics and Astronomy, University of Delaware, Newark, DE, USA, [17]Department of Space and Plasma Physics, Royal Institute of Technology, Stockholm, Sweden, [18]Denali Scientific, Healy, AK, USA, [19]Department of Physics and Astronomy, Dartmouth College, Hanover, NH, USA

Abstract Data from the NASA Magnetospheric Multiscale mission are used to investigate asymmetric magnetic reconnection at the dayside boundary between the Earth's magnetosphere and the solar wind. High-resolution measurements of plasmas and fields are used to identify highly localized (~15 electron Debye lengths) standing wave structures with large electric field amplitudes (up to 100 mV/m). These wave structures are associated with spatially oscillatory energy conversion, which appears as alternatingly positive and negative values of $\mathbf{J} \cdot \mathbf{E}$. For small guide magnetic fields the wave structures occur in the electron stagnation region at the magnetosphere edge of the electron diffusion region. For larger guide fields the structures also occur near the reconnection X-line. This difference is explained in terms of channels for the out-of-plane current (agyrotropic electrons at the stagnation point and guide field-aligned electrons at the X-line).

1. Introduction

Magnetic reconnection is important for plasmas in near and deep space and in the laboratory (Burch & Drake, 2009). The process leading to reconnection involves explosive conversion of magnetic energy to heat and kinetic energy of charged particles. Here we show with data from the NASA Magnetospheric Multiscale (MMS) mission that the reconnection process at the dayside boundary of the magnetosphere is often associated with large electric field components of highly confined wave-like structures with characteristics of oblique quasi-electrostatic whistler waves. This result is very different from the lower-magnitude, widespread, quasi-static electric fields that are also found by observation and simulation to drive reconnection (Pritchett & Mozer, 2009; Shay et al., 2007).

For asymmetric reconnection, with different plasma and magnetic pressures on either side of a boundary, the X-line (which separates magnetic field lines with different topologies) and the electron stagnation region (which marks the deepest penetration of magnetosheath electrons) separate along the Earth-Sun line (Cassak & Shay, 2007). For symmetric reconnection, as in the geomagnetic tail, these regions coincide. As shown in this letter, strong energy conversion that is highly localized within the electron diffusion region (EDR) can occur at both the X-line and the electron stagnation region, and which region dominates depends on the guide field. Particle-in-cell simulations of one of the same events by Swisdak et al. (2017) show the development of the standing oblique whistler waves and the strong energy conversion they produce near the electron stagnation region. We note that localized strong energy conversion has also been reported from simulations by Zenitani et al. (2011) and Pritchett (2013).

2. Observations

The NASA MMS mission extends the experimental investigation of magnetic reconnection in the boundary regions of the Earth's magnetosphere to the electron scale (Burch, Moore, et al., 2016). The present study investigates the structure of the EDR for two reconnection events observed at the dayside magnetopause, one on 16 October 2015 (event 1) and the other on 8 December 2015 (event 2) (Burch, Torbert, et al., 2016; Burch & Phan, 2016). Both of these previous studies investigated electron distribution functions (DFs), currents, and electric fields in asymmetric reconnection, which is found at the dayside magnetopause. Asymmetry in magnetopause reconnection is caused by the high magnetic pressure and low plasma pressure on the magnetosphere side of the reconnection current layer and the lower magnetic pressure and higher plasma pressure on the magnetosheath side (Cassak & Shay, 2007). Figure 1i shows a sketch of the typical magnetic reconnection geometry at the magnetopause with estimated trajectories of MMS for events 1 and 2.

Event 1 had a very small guide field (magnetic field component out of the page) of B_M/B_L ~0.1 in boundary-normal coordinates (Denton et al., 2016; Sonnerup & Cahill Jr., 1967), while event 2 had a moderate guide field with $B_M/B_L \sim 1$. A previous study (Burch, Torbert, et al., 2016) showed that in event 1 strong energy conversion, as measured by $\mathbf{J} \cdot (\mathbf{E} + \mathbf{v_e} \times \mathbf{B}) > 0$ (or equivalently $\mathbf{J} \cdot \mathbf{E}' > 0$), occurred in the electron stagnation region (S in Figure 1i) but very little energy conversion occurred near the X-line (X in Figure 1i). It was shown further that the out-of-plane current associated with the energy conversion (J_M) was carried by crescent-shaped electron distributions as had been predicted (Chen et al., 2016; Hesse et al., 2014).

In contrast, in event 2 it was found that significant out-of-plane currents occurred both near the X-line and in the electron stagnation region (Burch & Phan, 2016). It was concluded that the guide field provided a channel for electron flow and the resulting out-of-plane current near the X-line that is not present for very small guide fields. Event 2 was further distinguished from event 1 in that the trajectory of the spacecraft constellation was approximately normal to the magnetospheric boundary as shown in Figure 1i.

Here we examine with the highest resolution available the electric field, currents, and electron DFs within the EDR for both events in order to determine the causes of magnetic field energy conversion and the resulting interconnection of magnetic fields and acceleration of particles. We find that the energy conversion is associated with highly confined intense standing wave structures that have certain characteristics that are consistent with oblique quasi-electrostatic whistler waves.

2.1. The 15 October 2015 Event

Event 1 was the subject of the paper by Burch et al. (2016), which identified the EDR in the electron stagnation region with electric field data averaged to the 30 ms time scale of the 3-D electron distributions. Also identified by Burch et al. (2016) were the crescent-shaped electron DFs in the plane perpendicular to **B** and their evolution to parallel crescents during the transition from closed to open magnetic field lines. For the current study we analyzed the highest-resolution electric field data (8,192 s^{-1}) combined with 7.5 ms electron DFs described by Rager et al. (2018). This higher-resolution analysis revealed the wave-like nature of the reconnection electric field, which resulted in an oscillatory $\mathbf{J} \cdot \mathbf{E}'$ structure. We show in Figures 1a–1f MMS data for a 450 ms time period beginning at 13:07:02.150 UT on 16 October 2015. Noted in Figure 1a are the approximate locations of the electron stagnation region and the X-line. The wave-like nature of the electric field, which was not shown by the 30 ms resolution data of Burch et al. (2016), is clearly represented by the higher-resolution data. Figure 1d shows $\mathbf{J} \cdot \mathbf{E}'$ obtained by using 30 ms average **E** as in the Burch et al. paper, which also showed a large positive value and an adjacent but small negative value.

Although $\mathbf{J} \cdot \mathbf{E}'$ is a scalar quantity, it is illustrative to show the separate contributions of the three components, which indicates that the energy conversion was mainly associated with the out-of-plane current J_M and the out-of-plane (or reconnection) electric field E_M. The wave spectrograms in Figures 1e and 1f show the highest intensities near the energy conversion peak with electromagnetic waves at low frequencies and broadband mostly electrostatic waves above 100 Hz with the highest intensities below F_{ce} (electron cyclotron frequency). Wave analysis shown later identifies these waves with the whistler mode.

Figures 1g and 1h show vector electric field measurements for MMS2 and MMS3 zoomed in to the 130 ms interval noted by the red bar between Figures 1f and 1g. Based on the very similar electric field patterns in

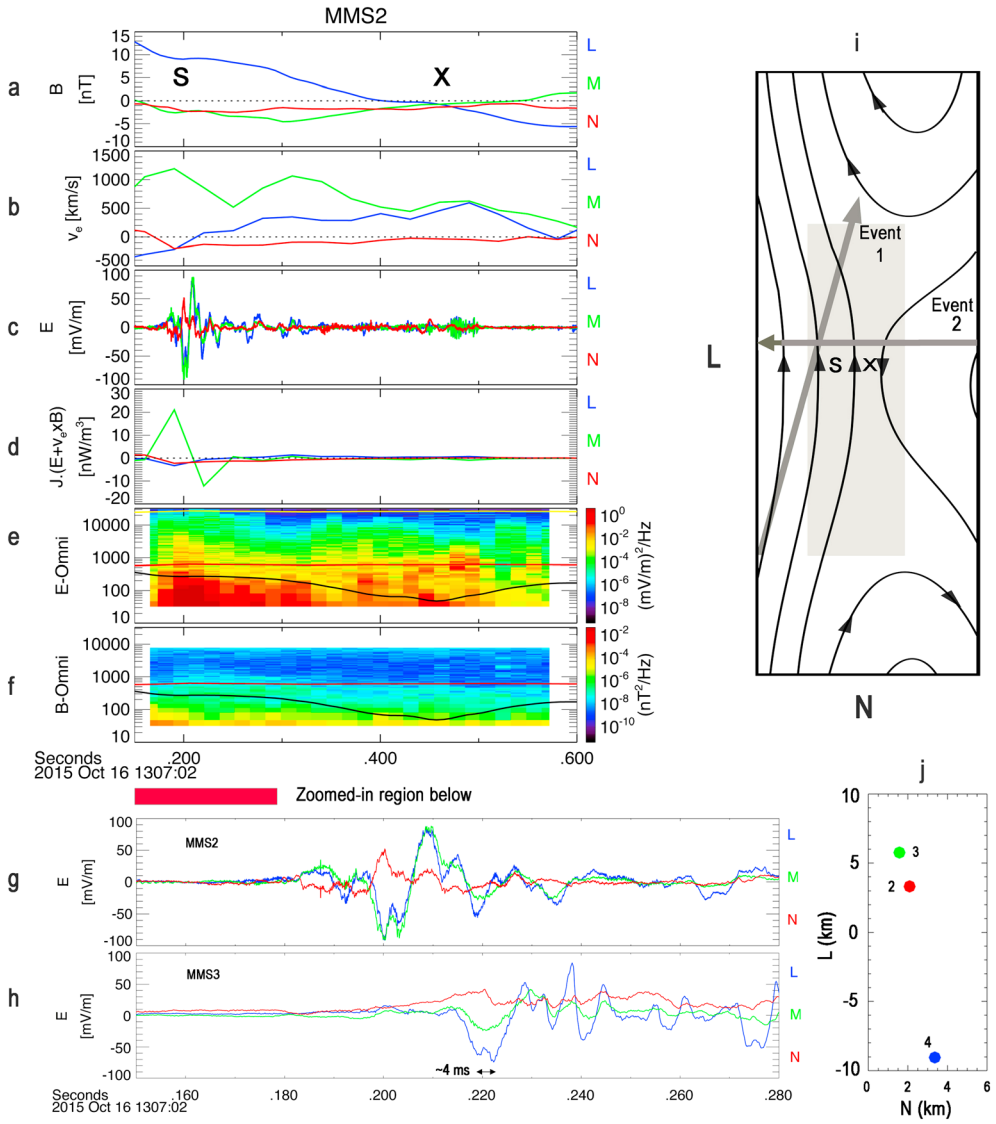

Figure 1. Plasma and field data for a reconnection event at the Earth's magnetopause on 16 October 2015. (a) Magnetic field with approximate S (stagnation region) and X (X-line) noted. (b) Electron velocity. (c) Electric field at 8,192 s^{-1}. (d) Energy conversion rate in plasma rest frame averaged to the 30 ms electron measurement cadence. (e) Electric power spectral density with F_{ce} (black curve) and F_{pi} (ion plasma frequency, red curve). (f) Magnetic power spectral density. (g) Zoomed-in vector electric field from MMS2 at the 8,192 s^{-1} E-field measurement cadence. (h) Same for MMS3. (i) Sketch of magnetic field lines for asymmetric reconnection with shaded region for electron diffusion region and gray arrow for spacecraft trajectories for events 1 and 2 with S and X denoting electron stagnation region and reconnection X-line, respectively. (j) Positions of MMS2, 3, and 4 for zoomed-in data period. All plots are in boundary-normal coordinates with transformation matrices from GSE (Geocentric Solar Ecliptic) to LMN coordnates: L = [0.31147, 0.02399, 0.94998]GSE, M = [0.48027, −0.8652, −0.13562]GSE, N = [0.81863, 0.49849, −0.28099]GSE (Denton et al., 2016).

Figures 1g and 1h and the ~0.5 km separation in N between MMS2 and MMS3 shown in Figure 1j, we deduce that the current layer separating the magnetosphere from the magnetosheath moved earthward at a velocity estimated to be ~30 km/s, causing the two spacecraft to traverse the electron stagnation region and the boundary between open and closed field lines in quick succession. This inward motion was accompanied by a faster southward motion causing the four MMS spacecraft (which were moving much slower at a few kilometers per second) to follow the approximate trajectory shown in Figure 1i. This trajectory is consistent with that derived for this event by Denton et al. (2016) and Hasegawa et al. (2017).

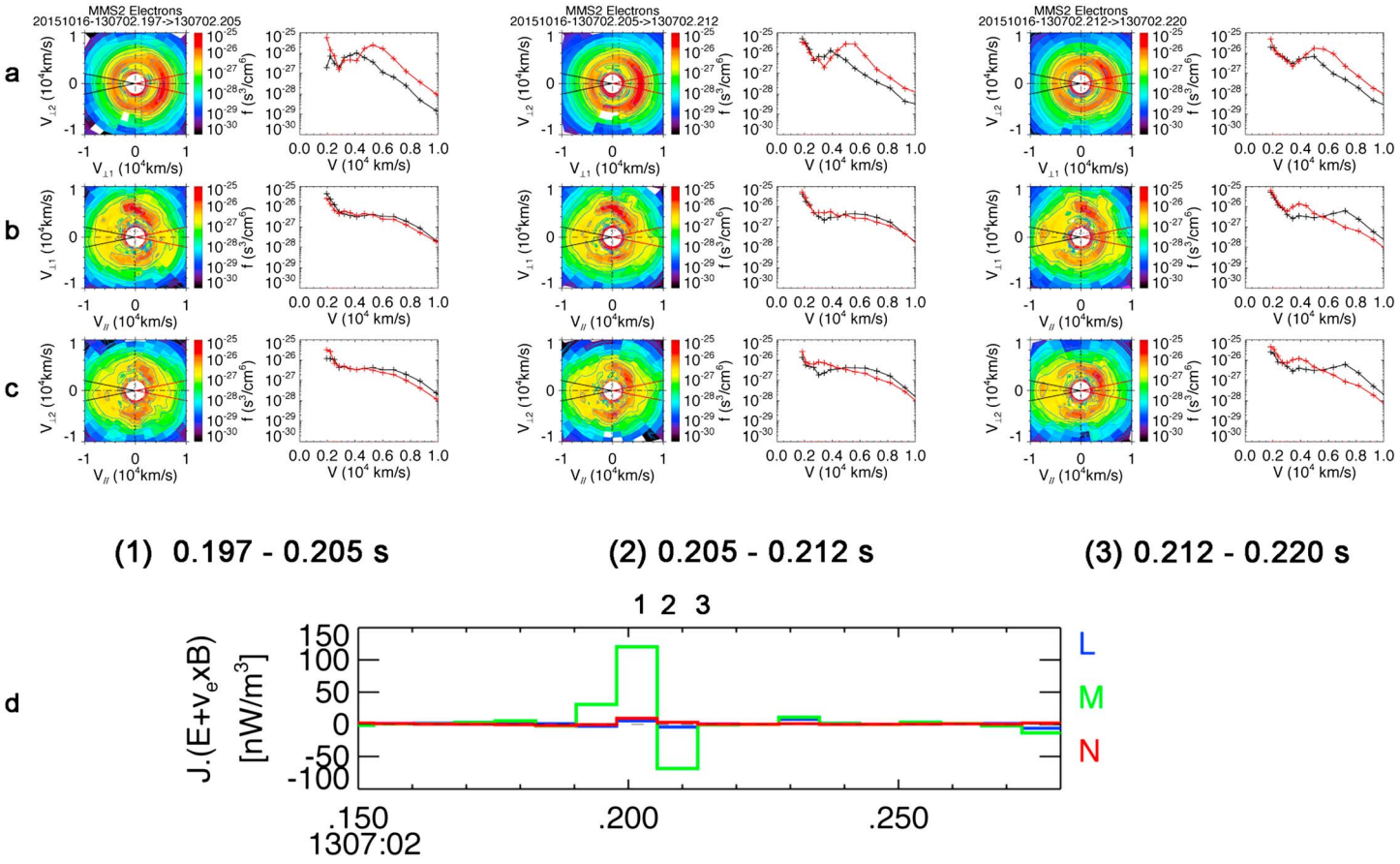

Figure 2. Electron distribution functions and energy conversion rate for a 130 ms period on 16 October 2015. (a) Electron distribution functions every 7.5 ms in the plane perpendicular to **B**. $v_{\perp 1}$ is in the (**b** × **v**) × **b** direction. $V_{\perp 2}$ is in the **E** direction. (b) Electron distribution functions in the plane containing **B** and $v_{\perp 1}$. (c) Electron distribution functions in the plane containing **B** and $v_{\perp 2}$. Line plots in b and c show average distribution function within the red and black sectors in each polar plot. (d) Energy conversion rate in plasma rest frame every 7.5 ms.

Evident in the measurements in Figures 1g and 1h are mostly positive boundary-normal electric fields (E_N) and bipolar parallel (E_L) and out-of-plane (E_M) electric fields with nearly equal magnitudes as in an oblique electrostatic wave. This wave structure, which for MMS2 has an amplitude >80 mV/m, was accompanied by out-of-plane currents (J_M) of about 10^{-6} amp/m^2 carried by electrons with crescent-shaped distributions (Burch, Torbert, et al., 2016; Hesse et al., 2014). Thus, the energy conversion rate in the negative E_M half of the wave structure was >80 nW/m^3 as is discussed further in connection with Figure 2. These E-fields are about 2 orders of magnitude greater than predicted reconnection electric fields (Cassak et al., 2017; Shay et al., 2016). However, the facts that (1) they exist over a distance (~0.5 km) less than the skin depth (c/ω_{pe}) and (2) they are bipolar in nature cause the average E_M over these characteristic electron scales to match more closely the expectations. We also note that the E_L and E_M signals exhibit a bifurcation with temporal width approximately equal to the cyclotron period (4 ms in Figure 1h), which may imply that the waves are amplified by electrons that are trapped by the parallel electric field components (Kellogg et al., 2010). We suggest a similar amplification for the events observed in the 16 October 2015 MMS event. We note in Figure 1c that the wave structure appears to propagate into the open field line region toward the X-line although it is possible that these are spatial structures left behind as the magnetopause moved earthward.

Electron DFs shown in Figure 2 show that the magnetic field line topology changed from closed to open over a 0.5 km structure containing the large oscillating electric fields. The polar plots of electron DFs in Figures 2a–2c are accompanied by line plots for measurements within the black and red sectors noted in the polar plots. For all three times plotted the line plots in the top row, which are in the plane perpendicular to **B**, show magnetosheath electrons mixed with magnetospheric electrons in crescent distributions. Figures 2b–2c show

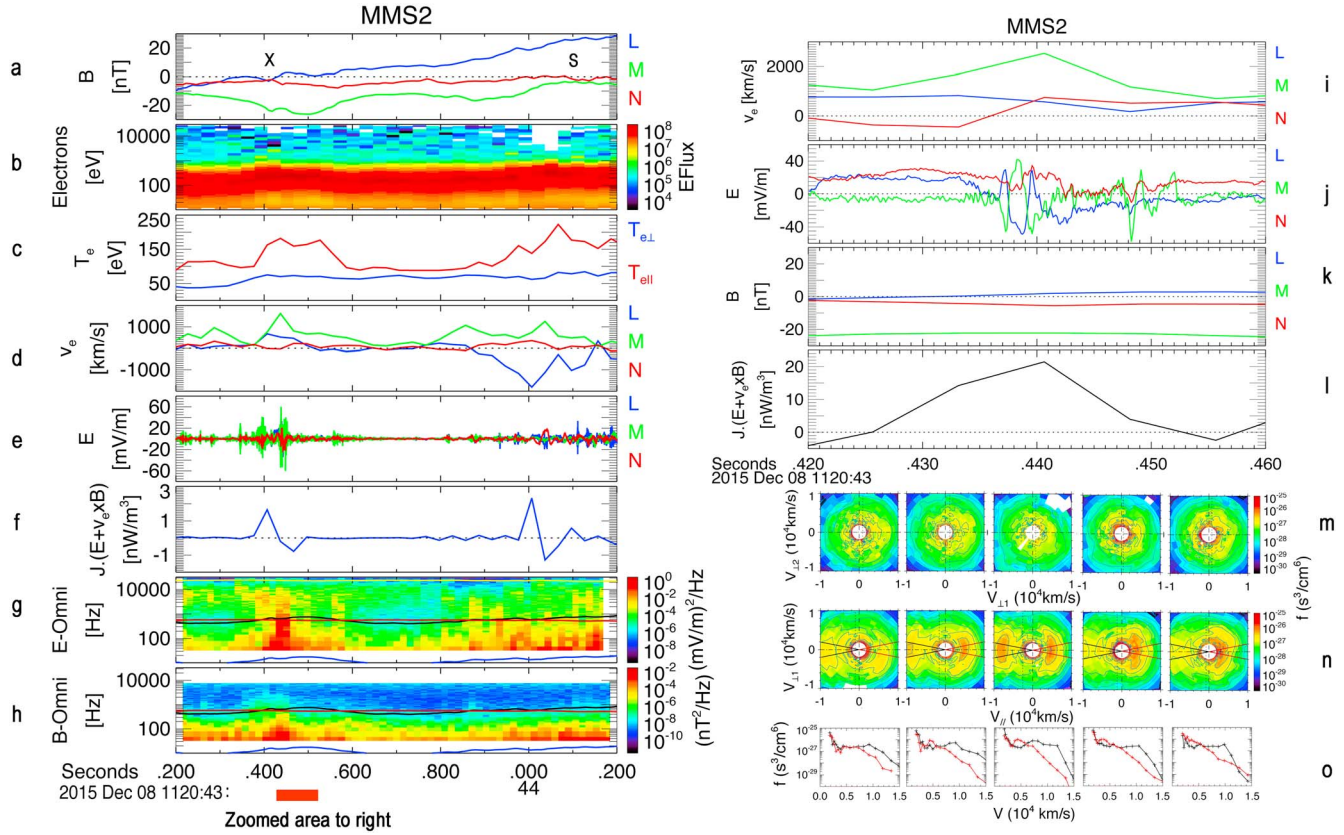

Figure 3. (left column) Plasma and field data on 8 December 2015. (a) Magnetic field. (b) Omnidirectional energy time electron spectrogram. (c) Electron temperature. (d) Electron velocity every 30 ms. (e) Electric field. (f) Energy conversion in plasma rest frame. (g) Electric power spectral density with F_{lh} (lower hybrid frequency, blue curve), F_{ce} (black curve), F_{pi} (red curve). (h) Magnetic power spectral density. (right column) Data zoomed in to the 40 ms period shown by the red bar at bottom of left panel. (i) Electron velocity every 7.5 ms. (j) Electric field. (k) Magnetic field. (l) $\mathbf{J} \cdot (\mathbf{E} + \mathbf{v_e} \times \mathbf{B})$ at 7.5 ms resolution. (m) Electron distribution functions every 7.5 ms in the plane perpendicular to **B** at times corresponding to the center of each plot. (n) Electron DFs every 7.5 ms in the plane containing **B** and $v_{\perp 1}$. (o) Cuts through the DFs in panel n with the black and red curves averaged over the black and red velocity sectors, respectively. Transformation matrices from GSE to LMN coordinates: L = [0.364074410, 0.071052083, 0.928655710]GSE, M = [−0.022889708, −0.996102090, 0.085186237]GSE, N = [0.931088550, −0.052270787, −0.361028920]GSE.

magnetic field-aligned electrons. For time (1) fluxes along +B and −B are nearly equal with a broad peak indicating more energetic magnetospheric electrons counterstreaming along the field. At time (3) the red and black curves are clearly different, showing a mixture of magnetosheath (red) and magnetospheric (black) electrons indicating open field lines. Time (2) shows an intermediate case between (1) and (3). The polar DF plots at times (2) and (3) show parallel crescent distributions as reported earlier by Burch et al. (2016). Figure 2d shows that the energy conversion rate peaks at time (1) and that it results in the breaking and reconnection of magnetic field lines as the closed field lines convert to open field lines at times (2) and (3). The energization of magnetosheath electrons associated with reconnection is shown by the difference between the black and red DF line plots in Figure 2a. The accelerated electrons have velocities along $v_{\perp 1}$ (the crescent direction), and this velocity is along the M direction as shown in Figure 1b.

2.2. The 8 December 2015 Event

Figure 3 plots similar data from MMS2 for event 2. Figures 3a–3f show that, in contrast to event 1, for this moderate guide field case there were large electron velocities in the M direction both near X and S, as noted before (Burch & Phan, 2016; Genestreti et al., 2017). Figures 3i–3o show zoom data for the 40 ms interval denoted by the red bar below Figure 3h. In this case v_e is plotted at 7.5 ms time resolution (Rager et al., 2018), showing a peak coincident with the strong electric field signal in Figure 3j, which has characteristics similar to those shown in Figures 1g–1h with a positive B_N signal accompanied by bipolar L and M

components. Figure 3k shows the reversal of B_L near a minimum of B_N, which is indicative of an in-plane null and X-line. The green curve in Figure 3k shows the guide field. Figure 3l shows the energy conversion rate, while Figures 3n, 3m, and 3o show the effects on the electron DFs. Both before and after the oscillating electric field structure or standing wave (at 0.437–0.440 s) the magnetic field lines are open, as indicated by the off-scale (yellow) extension in the $-v_{\|}$ direction. This extension is from magnetospheric electrons resulting from the connection of the field lines to the Northern Hemisphere. The lower-energy red regions in the polar DF plots indicate magnetosheath electrons moving along $+v_{\|}$. This mixture of magnetospheric and magnetosheath plasmas is shown better by the DF cuts in Figure 3o where the red and black line plots are average DF values within the red and black velocity sectors shown in Figure 3n (similar to the corresponding plots in Figure 2b).

Near 0.440 s, centered on the whistler wave structure, there is a red area along $v_{\|} < 0$ in Figure 3n, indicating an accelerated electron beam along the magnetic field, which is essentially the guide field. This beam is also shown by the black DF line plots in Figure 3o. At this point, the reconnection electric field is E_{-M} and the out-of-plane current is J_{-M}. As shown in Figure 3l, there is energy conversion leading to X-line reconnection at this point. As for event 1, the energization of magnetosheath electrons can be seen in the agyrotropic distributions in the perpendicular plane shown in Figure 3m. However, for this moderate guide field case Figures 3n and 3o show stronger acceleration as observed by the parallel beam along the guide field. The fact that there are open field lines on either side of the X-line is consistent with the diagram in Figure 1 with the spacecraft passing just north of the X-line. Referring to the middle plot in Figure 3n, the strong electron beam along $-v_{\|}$, being more energetic than the opposite beam along $+v_{\|}$, is responsible for carrying the out-of-plane current and results from the reconnection electric field, which is mostly E_{par} in this region. These conditions are consistent with current ideas about reconnection except for the important difference that they occur in a very restricted region of the EDR (smaller than the skin depth and the electron gyroradius) and involve electric fields 2 orders of magnitude larger than predicted ($<$1 mV/m), for example, by Cassak et al. (2017). Correspondingly, the $\mathbf{J} \cdot \mathbf{E}$ values are factors of 30 larger than predicted ($<$4 nW/m^3), also by Cassak et al. (2017).

3. Wave Analysis

An important issue to address is the nature and origin of the localized large oscillatory electric fields. The observation of similar wave forms with decreasing amplitudes downstream of the intense events observed by both MMS2 and MMS3 on 16 October 2015 (Figures 1g and 1h) and by MMS2 on 8 December 2015 (Figure 3j) could be interpreted as the propagation of waves from the electron stagnation region into the exhaust region. This observation could also be interpreted as the encounter of residual spatial structures left behind by the earthward motion of the magnetopause and reconnection current layer on 16 October 2015 and their sunward motion on 8 December 2015.

In order to shed more light on the nature of the oscillatory electric fields and the associated very small magnetic field fluctuations, wave analysis has been performed for event 1 (Figure 4a) and event 2 (Figure 4b). In both cases, within the frequency range containing the major wave structure, obliquely propagating waves are determined by Poynting flux analysis, and hodograms show elliptically polarized waves with generally right-hand polarization. In addition to the major structures, where for event 1 the duration is about 20 ms and for event 2 the duration is about 3 ms, there are superimposed higher-frequency oscillations with much smaller amplitudes. In order to eliminate these higher-frequency signals from the analysis, we focus on frequency ranges for each event in which we expect whistler waves to exist (near half the electron cyclotron frequency). These ranges are 75 to 125 Hz for event 1 and 300 to 500 Hz for event 2.

Hodograms are shown in Figures 4c–4e with an asterisk noting the starting point and arrows showing the direction of rotation. The oscillations observed for event one (Figure 4c) are right handed in the electric field. For the magnetic field, the polarization changes from right handed to mostly linear and then back to right handed. However, taking note of the difference in the magnitudes of the oscillations ($E \sim 25$ mV/m, $B \sim 0.02$ nT, $E/B > 10^8$), this wave is quasi-electrostatic and as such the electric field oscillations are more important. Because of the obliquity of the wave packet, this wave is likely propagating along the resonance cone and as such has mode converted into a quasi-electrostatic whistler wave, consistent with theory (Kumar et al., 2017).

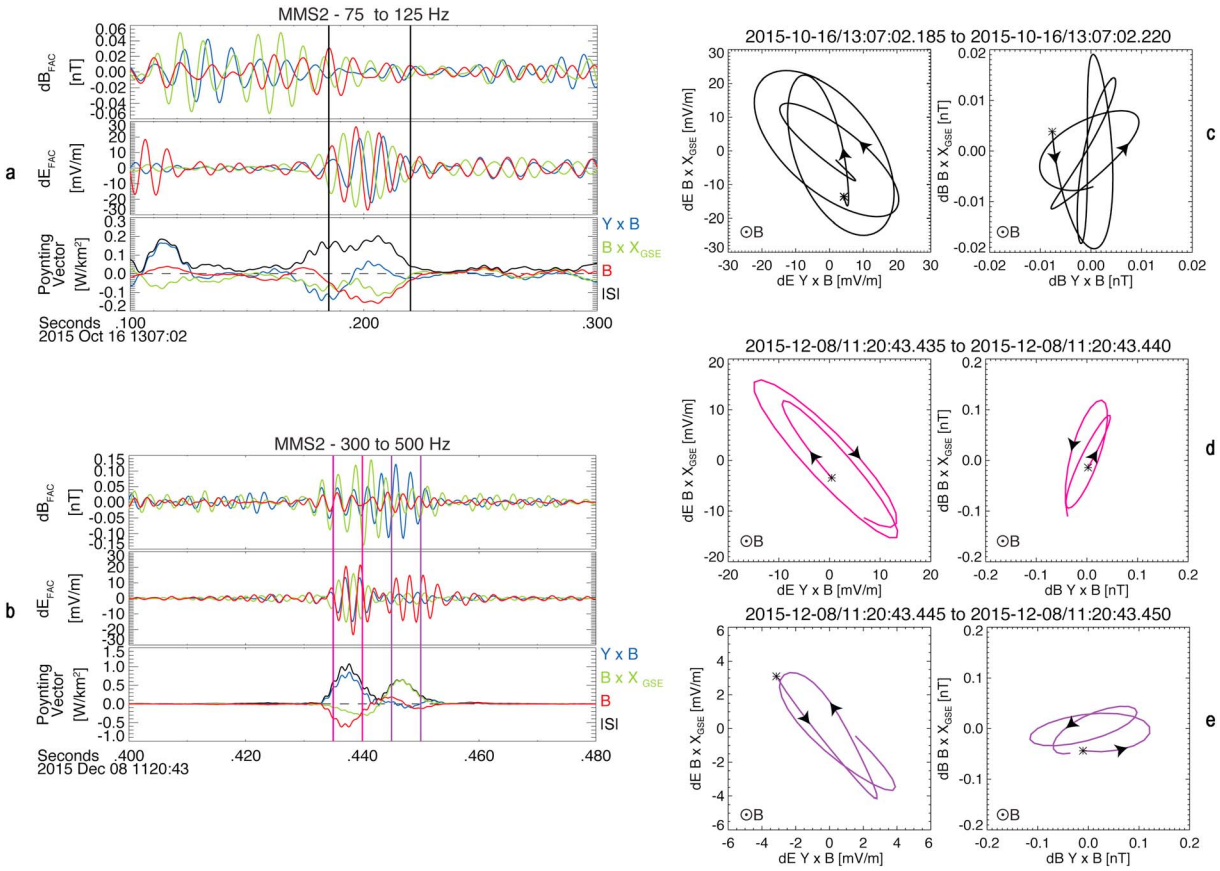

Figure 4. (a) **E** and **B** wave fields and Poynting vector in magnetic field-aligned coordinates filtered to 75–125 Hz for event 1 on 16 October 2015. (b) Same as panel a but for 8 December 2015 at 300–500 Hz. (c) **E** and **B** hodograms for time period bounded by the two vertical lines in panel a with the starting point noted by an asterisk and the rotation direction by the arrowheads. (d) Same as panel c except for the time period bounded by the two magneta vertical lines in panel b. (e) Same as panel d except for the time period bounded by the two purple vertical lines.

For event 2 two distinct wave packets are observed near the region of interest. The start and stop times of these wave packets are noted by the magenta and purple vertical lines in Figure 4b. The first wave packet observed before 11:20:43.440 UT, marked by the magenta lines, is found to be right handed for the B-field oscillations and left handed for the E-field oscillations. The second wave packet, observed after 11:20:43.440 UT, marked by purple vertical lines, is shown to be right handed for both the E-field and B-field oscillations, consistent with whistler waves. This change in E-field polarization could possibly be an effect of reflection of the wave packet (note that the Poynting vector direction of the two wave packets is in different directions), which would give possible evidence of a standing wave or source region.

We investigated the observed electron DFs as possible sources of the large oblique whistler-like oscillations with inconclusive results. For example, the parallel beams shown in Figures 2c and 3n were not found to generate oblique whistler mode waves, as might be expected from the relatively high beta (>5) in the two events (e.g., Sauer & Sydora, 2010). Another consideration is the small width of the events, which are only 15–20 Debye lengths and only marginally larger than the theoretical limit of $2\pi\lambda_D$ for the shortest wavelength that can occur in a plasma. Thus, it is possible that these are Debye-scale solitary structures rather than standing oblique whistler waves (e.g., Ergun et al., 1998), and more analysis is clearly needed to determine definitively the nature and cause of these large oscillatory structures, which are associated with conversion of electromagnetic energy to particle energy in the EDR.

4. Conclusions

We have shown with MMS data that reconnection energy conversion at the Earth's dayside magnetopause occurs in highly localized regions within the EDR. For an event with a very small guide magnetic field the

only significant energy conversion was located near the electron stagnation region, while for an event with guide field ~1 significant energy conversion occurred both near the X-line and near the stagnation region. The general result that energy conversion near the X-line depends on significant guide field has been described by Genestreti et al. (2017). We have shown further that the energy conversion is associated with an oscillatory electric field pattern that shows characteristics of both a spatial structure and a propagating wave. We showed by wave analysis that the events are most likely standing oblique quasi-electrostatic whistler waves. The oscillating electric fields, combined with fairly uniform out-of-plane currents, lead to alternating positive and negative $\mathbf{J} \cdot \mathbf{E}'$ values with the positive values associated with the conversion of electromagnetic energy to particle energy and the negative values indicating conversion of particle energy to electromagnetic energy. By using the 7.5 ms electron distributions derived by Rager et al. (2018), we were able to show for the electron stagnation region of the 16 October 2015 event that the positive $\mathbf{J} \cdot \mathbf{E}'$ peak corresponded exactly with the conversion of closed to open magnetic field lines. It was further shown for the 8 December 2015 event that the peak positive $\mathbf{J} \cdot \mathbf{E}'$ value aligned with the appearance of a strong electron beam along the boundary-normal M direction producing the out-of-plane current of reconnection.

Swisdak et al. (2017) show by plasma simulation the development of structures they identify as standing oblique whistler waves for parameters derived from the 16 October 2015 event we have described. In their simulation the standing oscillatory structure is generated by electrons streaming along the outer reconnection separatrix that are accelerated through the magnetic null region toward the electron stagnation regions by a strong E_N component. They find both positive and negative values of $\mathbf{J} \cdot \mathbf{E}$ associated with electric field amplitudes up to 25 mV/m. Within the limitations of the PIC simulation, these results are consistent with the MMS observations.

Acknowledgments

This work was supported by NASA contract NNG04EB99C at SwRI. The entire MMS data set is available online at https://lasp.colorado.edu/mms/sdc/public/links/. Fully calibrated data are placed online at this site within 30 days of their transmission to the MMS Science Operations Center. The data are archived in the NASA Common Data Format (CDF) and so can be plotted using a number of different data display software packages that can use CDF files. A very comprehensive system called the Space Physics Environment Data Analysis System (SPEDAS) is available by downloading http://themis.ssl.berkeley.edu/socware/bleeding_edge/ and selecting spdsw_latest.zip. Training sessions on the use of SPEDAS are held on a regular basis at space physics-related scientific meetings. All of the data plots in this paper were generated with SPEDAS software applied to the publicly available MMS database, so they can readily be duplicated.

References

Burch, J. L., & Drake, J. F. (2009). Reconnecting magnetic fields. *American Scientist*, *97*(5), 392–299. https://doi.org/10.1511/2009.80.392

Burch, J. L., Moore, T. E., Torbert, R. B., & Giles, B. L. (2016). Magnetospheric Multiscale overview and science objectives. *Space Science Reviews*, *199*(1-4), 5–21. https://doi.org/10.1007/s11214-015-0164-9

Burch, J. L., & Phan, T. D. (2016). Magnetic reconnection at the dayside magnetopause: Advances with MMS. *Geophysical Research Letters*, *43*, 8327–8338. https://doi.org/10.1002/2016GL069787

Burch, J. L., Torbert, R. B., Phan, T. D., Chen, L. J., Moore, T. E., Ergun, R. E., et al. (2016). Electron-scale measurements of magnetic reconnection in space. *Science*, *352*(6290), aaf2939. https://doi.org/10.1126/science.aaf2939

Cassak, P. A., Genestreti, K. J., Burch, J. L., Phan, T. D., Shay, M. A., Swisdak, M., et al. (2017). The effect of a guide field on local energy conversion during asymmetric magnetic reconnection: Particle-in-cell simulations. *Journal of Geophysical Research: Space Physics*, *122*, 11,523–11,542. https://doi.org/10.1002/2017JA024555

Cassak, P. A., & Shay, M. A. (2007). Scaling of asymmetric magnetic reconnection: General theory and collisional simulations. *Physics of Plasmas*, *14*(10), 102114. https://doi.org/10.1063/1.2795630

Chen, L.-J., Hesse, M., Wang, S., Gershman, D., Ergun, R., Pollock, C., et al. (2016). Electron energization and mixing observed by MMS in the vicinity of an electron diffusion region during magnetopause reconnection. *Geophysical Research Letters*, *43*, 6036–6043. https://doi.org/10.1002/2016GL069215

Denton, R. E., Sonnerup, B. U. Ö., Hasegawa, H., Phan, T. D., Russell, C. T., Strangeway, R. J., et al. (2016). Motion of the MMS spacecraft relative to the magnetic reconnection structure observed on 16 October 2015 at 1307 UT. *Geophysical Research Letters*, *43*, 5589–5596. https://doi.org/10.1002/2016GL069214

Ergun, R. E., Carlson, C. W., McFadden, J. P., Mozer, F. S., Muschietti, L., Roth, I., & Strangeway, R. J. (1998). Debye-scale plasma structures associated with magnetic-field-aligned electric fields. *Physical Review Letters*, *81*(4), 826–829. https://doi.org/10.1103/PhysRevLett.81.826

Genestreti, K. J., Burch, J. L., Cassak, P. A., Torbert, R. B., Ergun, R. E., Varsani, A., et al. (2017). The effect of a guide field on local energy conversion during asymmetric magnetic reconnection: MMS observations. *Journal of Geophysical Research, Space Physics*, *122*, 11,342–11,353. https://doi.org/10.1002/2017JA024247

Hasegawa, H., Sonnerup, B. U. Ö., Denton, R. E., Phan, T. D., Nakamura, T. K. M., Giles, B. L., et al. (2017). Reconstruction of the electron diffusion region observed by the Magnetospheric Multiscale spacecraft: First results. *Geophysical Research Letters*, *44*, 4566–4574. https://doi.org/10.1002/2017GL073163

Hesse, M., Aunai, N., Sibeck, D., & Birn, J. (2014). On the electron diffusion region in planar, asymmetric, systems. *Geophysical Research Letters*, *41*, 8673–8680. https://doi.org/10.1002/2014GL061586

Kellogg, P. J., Cattell, C. A., Goetz, K., Monson, S. J., & Wilson, L. B. III (2010). Electron trapping and charge transport by large amplitude whistlers. *Geophysical Research Letters*, *37*, L20106. https://doi.org/10.1029/2010GL044845

Kumar, S., Sharma, R. P., Moon, Y. J., & Goyal, R. (2017). Quasi-electrostatic whistler wave dynamics in Earth's radiation belt. *The Astrophysical Journal*, *851*(1), 6. https://doi.org/10.3847/1538-4357/aa9716

Pritchett, P. L. (2013). The influence of intense electric fields on three-dimensional asymmetric magnetic reconnection. *Physics of Plasmas*, *20*(6), 061204. https://doi.org/10.1063/1.4811123

Pritchett, P. L., & Mozer, F. S. (2009). The magnetic field reconnection site and dissipation region. *Physics of Plasmas*, *16*(8), 080702. https://doi.org/10.1063/1.3206947

Rager, A. C., Dorelli, J. C., Gershman, D. J., Uritsky, V., Avanov, L. A., Torbert, R. B., et al. (2018). Electron crescent distributions as a manifestation of diamagnetic drift in an electron-scale current sheet: Magnetospheric Multiscale observations using new 7.5 ms Fast Plasma Investigation moments. *Geophysical Research Letters*, *45*. https://doi.org/10.1002/2017GL076260

Sauer, K., & Sydora, R. D. (2010). Beam-excited whistler waves at oblique propagation with relation to STEREO radiation belt observations. *Annales de Geophysique*, *28*(6), 1317–1325. https://doi.org/10.5194/angeo-28-1317-2010

Shay, M. A., Drake, J. F., & Swisdak, M. (2007). Two-scale structure of the electron dissipation region during collisionless magnetic reconnection. *Physical Review Letters*, *99*(15), 155002. https://doi.org/10.1103/PhysRevLett.99.155002

Shay, M. A., Phan, T. D., Haggerty, C. C., Fujimoto, M., Drake, J. F., Malakit, K., et al. (2016). Kinetic signatures of the region surrounding the X line in asymmetric (magnetopause) reconnection. *Geophysical Research Letters*, *43*, 4145–4154. https://doi.org/10.1002/2016GL069034

Sonnerup, B. U. Ö., & Cahill, L. J. Jr. (1967). Magnetopause structure and attitude from *Explorer 12* observations. *Journal of Geophysical Research*, *72*(1), 171–183. https://doi.org/10.1029/JZ072i001p00171

Swisdak, M., Drake, J. F., Price, L., Burch, J. L., Cassak, P. A., & Phan, T. D. (2017). Localized and intense energy conversion in the diffusion region of asymmetric magnetic reconnection, ArXiv: 1710.04555.

Zenitani, S., Hesse, M., Klimas, A., & Kuznetsova, M. (2011). New measure of the dissipation region in collisionless magnetic reconnection. *Physical Review Letters*, *106*(19), 195003. https://doi.org/10.1103/PhysRevLett.106.195003